AGU ADVANCING EARTH AND SPACE SCIENCE

Geophysical Research Letters®

RESEARCH LETTER
10.1029/2022GL101150

High and Dry: Billion-Year Trends in the Aridity of River-Forming Climates on Mars

Edwin S. Kite[1] **and Axel Noblet**[2,3]

[1]University of Chicago, Chicago, IL, USA, [2]Nantes Université, LPG-CNRS-UMR6112, Nantes, France, [3]University of Western Ontario, London, ON, Canada

Key Points:

- Aridity on Mars increased over time, but intermittently wetter climates persisted in lowlands
- Consistent with a change in Mars' greenhouse effect that left highlands too cold for liquid water except during a brief melt season
- Data are consistent with switch, of unknown cause, in dependence of aridity index on elevation: high-and-wet early on, high-and-dry later

Supporting Information:

Supporting Information may be found in the online version of this article.

Correspondence to:

E. S. Kite,
kite@uchicago.edu

Citation:

Kite, E. S., & Noblet, A. (2022). High and dry: Billion-year trends in the aridity of river-forming climates on Mars. *Geophysical Research Letters*, *49*, e2022GL101150. https://doi.org/10.1029/2022GL101150

Received 4 SEP 2022
Accepted 18 NOV 2022

Author Contributions:

Conceptualization: Edwin S. Kite
Formal analysis: Edwin S. Kite
Funding acquisition: Edwin S. Kite
Investigation: Edwin S. Kite
Methodology: Edwin S. Kite
Resources: Edwin S. Kite, Axel Noblet
Software: Edwin S. Kite
Visualization: Edwin S. Kite, Axel Noblet
Writing – original draft: Edwin S. Kite
Writing – review & editing: Edwin S. Kite, Axel Noblet

Abstract Mars' wet-to-dry transition is a major environmental catastrophe, yet the spatial pattern, tempo, and cause of drying are poorly constrained. We built a globally distributed database of constraints on Mars late-stage paleolake size relative to catchment area (aridity index (AI)), and found evidence for climate zonation as Mars was drying out. Aridity increased over time in southern midlatitude highlands, where lakes became proportionally as small as in modern Nevada. Meanwhile, intermittently wetter climates persisted in equatorial and northern-midlatitude lowlands. This is consistent with a change in Mars' greenhouse effect that left highlands too cold for liquid water except during a brief melt season, or alternatively with a fall in Mars' groundwater table. The data are consistent with a switch of unknown cause in the dependence of AI on elevation, from high-and-wet early on, to high-and-dry later. These results sharpen our view of Mars' climate as surface conditions became increasingly stressing for life.

Plain Language Summary Mars' surface was habitable in the past but is sterile today. Mars had multiple lake-forming eras as the planet dried out, but so far, there has been no globally distributed survey of the size of late-stage lakes, and the evaporation/precipitation ratio (aridity index (AI)) of the climates that formed them. This is key input/test data for models of Mars' past climate and climate evolution. We built a globally distributed database of AI constraints for late-stage river-forming climates on Mars. On average, late-stage lake-forming climates had a higher aridity than early-stage river-forming climates. Drying-out was spatially heterogenous, with a "high-and-dry" pattern. This apparently contrasts with a "high-and-wet" pattern seen for early-stage river-forming climates. The reasons for this apparent switch are unknown.

1. Introduction

Today Mars is a cold desert, but billions of years ago Mars had rivers and lakes. Early on, during the Late Noachian/Early Hesperian (~3.6 Ga), water supply to crater lakes was large enough relative to evaporation that—at least intermittently—liquid water overspilled to carve canyons (Fassett & Head, 2008). Later, runoff continued intermittently for ≳1 Gyr (e.g., Grant & Wilson, 2011; Holo et al., 2021; Kite, 2019), forming deltas and alluvial fans (e.g., Grant & Wilson, 2011; Salese et al., 2019) that were probably precipitation-fed (Kite, 2019), but these features were patchy (Wilson et al., 2021), with relatively few aqueous minerals visible from orbit (Pan et al., 2021), and lake overspills were less frequent (Goudge et al., 2016). At least some of the delta materials to be returned to Earth from Jezero crater likely date from the later era (e.g., Mangold et al., 2020; Salese et al., 2020). The data suggest a shift over time to wet events that were more short-lived, and/or to more arid climates. During this period, Mars was losing both CO_2 and H_2O, and the rate of asteroid impacts had declined to near-modern levels, yet volcanism and chaotic large-amplitude obliquity change continued (Haberle et al., 2017). Understanding the cause of changing lake levels is key to understanding the habitable-to-uninhabitable transition of Mars' surface environment, but the change itself is, as yet, poorly quantified.

To understand Mars' wet-to-dry transition, we need to know trends over time in mean aridity, and the spatial distribution of aridity. Past aridity (specifically, aridity index (AI), the ratio of potential evaporation to precipitation) can be constrained using paleolake size. The topographic catchment area feeding into the lake divided by paleolake size (the hydrologic X-ratio, X_H) is, in hydrological steady state, approximately equal to the climatic AI. This is because water from the topographic catchment is routed into a small area (the lake), and evaporation from the basin is reduced in proportion to the smallness of the lake (Matsubara & Howard, 2009). Following (e.g.) Stucky de Quay et al. (2020), we assume that all meltwater/rainwater is routed to the lake, infiltration is minor, the lake level is in hydrologic steady state, and runoff production on the lake itself is small (so that

X_H = (topographic catchment area not including lake area)/lake area). AI constrains paleoclimate models (e.g., Guzewich et al., 2021; Kamada et al., 2021; Kite et al., 2021; Turbet & Forget, 2021), and is a window into the evolution of ancient climate on Mars. Earlier-stage river-forming climates had X_H = 3–7 (Fassett & Head, 2008; Matsubara et al., 2011; Stucky de Quay et al., 2020), perhaps less (Matsubara et al., 2013). However, perhaps surprisingly, few estimates exist for how AI changed over time on Mars (e.g., Horvath & Andrews-Hanna, 2017), and there has been no previous survey of X_H for late-stage rivers/lakes.

In this study, we surveyed the interiors of all large, young craters (n = 212 areas) at latitudes between 40°N and 40°S mapped as Late Hesperian or Amazonian impacts (from Tanaka et al. (2014)). The purpose of the latitude cut was to minimize overprinting by ice-associated processes. We also surveyed seven additional craters that have relatively well-preserved rims, denoting relative youth, and defining closed basins. Well-preserved rims correspond to a closed catchment in most cases. The water-worn landforms within these craters formed during the Late Hesperian and Amazonian—extending >1 Gyr after the valley networks (e.g., Grant & Wilson, 2011). Many workers have argued that the wet events were probably intermittent (e.g., Kite, 2019, and references therein), with no rivers flowing for most of the time. Our results constrain conditions shortly before the last drying-out of low-latitude rivers on Mars. We then compared to work on early-stage rivers to find aridity trends over time.

2. Materials and Methods

To search for paleohydrologic proxies, we used Context Camera (CTX) data (Dickson et al., 2018; Malin et al., 2007), supplemented in a few places by High Resolution Imaging Science Experiment (HiRISE; McEwen et al., 2007) images. For topography, we used Mars Orbiter Laser Altimeter (MOLA) Precision Experimental Data Records (PEDRs; Smith et al., 2001), and in some places we used CTX/HiRISE DTMs (Mayer & Kite, 2016).

To constrain X_H, we need estimates of paleolake area, A, and drainage area, D ($X_H = (D - A)/A = D/A - 1$; Matsubara et al., 2011; Figure 1). Here, the "−1" corresponds to the assumption that no runoff is produced on the lake itself. To get paleolake area, thanks to the high quality of Mars topographic data (Smith et al., 2001) together with only minor postlacustrine modification, it is usually enough to know paleolake water level. However, water level changed over time and most geologic proxies for past water level on Mars are indirect, so these estimates are not precise and may correspond to only the maximum (highest) lake levels. From the water level, the contour-enclosed area corresponds to past lake area. Water level constraints include flat crater-bottom deposits (FCBDs) interpreted as playa/lake deposits, intrabasin spillways, and delta break-in-slope elevations. Upper-bound constraints come from the lowest (terminal) elevations of subaerial fans and channels, as these cannot form below lake level. For alluvial fan toes/channel termini, we used low-point elevations to draw an enclosing contour. The areas enclosed by these contours are upper limits on A. Many fans on Mars formed over long time scales (Kite et al., 2017), but channels can be carved rapidly (e.g., Whipple et al., 2000). Therefore, the X_H obtained from setting lake elevation equal to a channel-stop elevation (requiring that the lake level did not exceed the channel-stop elevation for at least as long as it took to carve the channel) constrains lake level over a shorter-time scale than the constraint obtained from a fan terminus elevation. (In figures, we mark the shorter-time scale channel-stop lower limits on X_H with red open triangles, and the longer-time scale fan toe lower limits on X_H with red filled triangles.) Wind erosion reduces lake deposit extent relative to original extent; we use lake deposit area as a lower limit on A. Internal spillways also provide lower limits on A. The slope-break elevation of deltas provides a best estimate of past lake level. For the deltas we analyzed, layer-orientation data was not available, so our assessment was based only on geomorphic expression (modern topography), which is less definitive than stratigraphic methods (e.g., Tebolt & Goudge, 2022). Our approach treats the present-day topographic relationships between lake deposit outcrops and alluvial fan deposit outcrops as being representative of the topographic relationships between deposits when the rivers were flowing. Infrequently, we observe FCBDs topographically above fan toes (e.g., at Luba crater), presumably due to differential wind erosion. At Peridier, channels extend topographically below the FCBDs that we interpret as lake deposits, perhaps corresponding to a later wet episode. At all sites, small channels were neglected. We recorded only the constraints that (within a given drainage area) were the most hydrologically constraining.

Drainage areas were taken to be the entire area of the host crater, except when internal drainage relations (ridges, spillways) showed a smaller contributing area. Some crater interiors contained multiple drainage areas, due to internal drainage divides, which were accounted for separately. We assume that all topographic drainage area (and

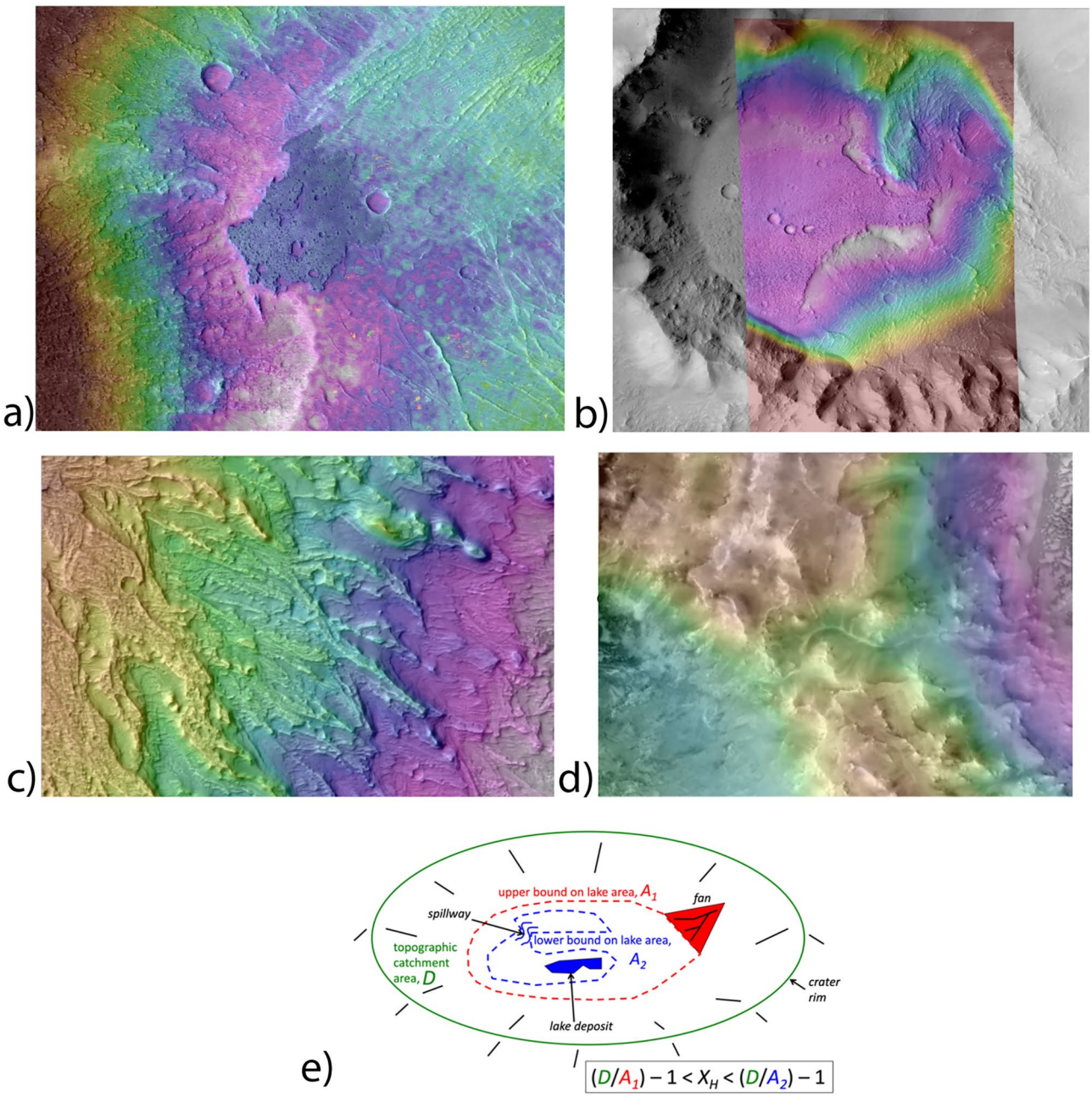

Figure 1. Examples of paleohydrologic proxies (for details, see Figures S1–S4 in Supporting Information S1). (a) Flat crater-bottom deposit (FCBD) interpreted as a lake/playa deposit. Image is ~10 km across. Elevation range 150 m. F10_039889_1567_XN_23S286W stereopair. 23°S 74°E. (b) Additional FCBD interpreted as a lake/playa deposit. Colored HiRISE DTM (ESP_065414_1495/ESP_065480_1495 stereopair) is 5.2 km across. Red-to-white elevation range is 200 m. The S rim of the impact crater has numerous erosional alcoves, linked by a depositional ramp to the FCBD. The depositional ramp is topped by sinuous ridges, one of which feeds into the FCBD. (c) Alluvial fan deposit (image is 5.5 km across, PSP_007688_1575/PSP_008545_1575 stereopair, elevation range 200 m). (d) Spillway (image is 29.7 km across, J15_050464_1996_XI_19N284W, elevation range 2,260 m). (e) Cartoon showing use of paleohydrologic proxy data to estimate *X*-ratio (X_H) within a crater 10s of km across. Dashed lines correspond to contours at the elevations of geologic features. Area within contours gives lake area estimate. Dividing topographic catchment area by lake area estimate gives $X_H + 1$.

not just the area upstream of observed channels) contributes water to the lake. If water was sourced by patchy snowmelt, then more runoff production per unit area would be needed.

Each proxy type has been described previously in detailed studies (e.g., Moore & Howard, 2005; Palucis et al., 2016). For example, flat-lying sediments interpreted as lake deposits are described by Grant et al. (2008)

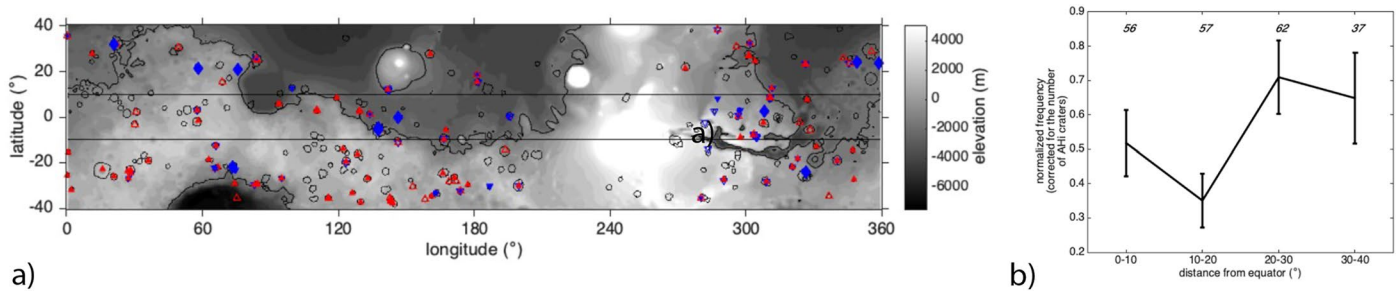

Figure 2. (a) Aridity survey map (see Figure S5 in Supporting Information S1 for details). Black contours locate young impact craters ("AHi" units from Tanaka et al. (2014)) inspected for paleohydrology constraints. Black lines: −1,500 m elevation contour and ±10° latitude lines. Blue triangles = FCBDs (interpreted as lake deposits; unfilled = candidate), blue diamonds = deltas/shorelines, blue circles = internal spillways, red filled triangles = alluvial fan toes, red unfilled triangles = channel-stops. (b) Distribution of frequency of craters with paleohydrologic evidence with distance from the equator (see Figure S6 in Supporting Information S1 for details). Vertical bars correspond to $\sqrt{N}$ uncertainty. Numbers in italics: per-bin sample size.

and Morgan et al. (2014). As far as we know, this is the first global survey for FCBDs that we interpret as lake deposits, so we provide more information on this proxy type below. Figures S1–S4 in Supporting Information S1 (and Figures 1a and 1b) show many-km-wide crater-bottom deposits that have an elevation range of only a few meters. FCBDs frequently have slopes of 1/1,000, 10–20× flatter than nearby alluvial fans. FCBDs lack channels, show pits and grooves due to wind erosion, are usually found downslope from alluvial fans, and are typically bounded by outward-facing scarps. Internal layering and susceptibility to wind erosion suggest that these are indurated sedimentary deposits. Extreme flatness and location at the bottom of a crater indicate that aggradation was controlled by an equipotential, most likely liquid water. In some cases (Figure S2a in Supporting Information S1), sinuous ridges that we interpret as capped by fluvial deposits connect to FCBDs (Davis et al., 2019), strengthening confidence in the lake-deposit interpretation of those FCBDs. HiRISE DTMs (Figures S2–S4 and S7 in Supporting Information S1) confirm these impressions and add detail on the gentle tilts of internal layers (typically $\lesssim 1°$, consistent with flat after tracing and DTM errors are taken into account). These dips are significantly lower than those typical for Mars sediments interpreted as topography-draping air fall deposits (Annex & Lewis, 2020). Sediments may have been transported into the lakes by either wind or water. Internal-layer conformity with deposit tops proves that flatness of deposit tops is not a chance of erosion but rather a trace of depositional process. Layers are expressed due to contrasts in erosional resistance, which in turn might relate to changes in grainsize or composition. Although no spectral confirmation of aqueous minerals is available in most cases, and therefore it remains conceivable that some of these FCBDs might be impact melt, we interpret these as lake deposits. (Unlike impact melts, cataloged FCBDs are flatter, and lack flow texture, arcuate ridges, and crumple ridges). When topographic data were lacking, we marked the deposit as a "candidate" FCBD. It is likely that some lake deposits are not interpretable from orbiter data (false negatives). The Murray mudstones at Gale, interpreted as lake deposits by Grotzinger et al. (2015), would not be counted this way.

3. Results of Survey: Latitude and Elevation Trends

Most craters show evidence for past liquid water ($n = 118$ basins; Figure 1). Presumably some craters lack evidence for liquid water because they postdate Mars' drying-out (Holo et al., 2021). Past lake size is constrained by the extent of FCBDs interpreted as lake/playa deposits (e.g., Morgan et al., 2014; $n = 87$ including 30 candidates; Figures S1–S4 in Supporting Information S1), as well as the elevations of features such as alluvial fan termini, channel termini, internal spillways, candidate shorelines, and the break-in-slope elevation of scarp-fronted deposits interpreted as deltas ($n = 135$; Figure 1).

Within craters, fans were built by flows from crater sidewalls, suggesting precipitation runoff was responsible for fluvial sediment transport (Lamb et al., 2006). Lake levels could have been maintained by water conveyed from crater sidewalls (by surface runoff or shallow groundwater flow) or alternatively, by deep-upwelling groundwater sourced from (e.g.) rain/melt recharge at $\sim 10^2$–10^3-km scales (Horvath & Andrews-Hanna, 2017; Salese et al., 2019). We do not think that the lakes were flooded by catastrophic release of groundwater (Wang et al., 2005), because channels run up to ridgelines and because only some places saw water. Figure 2a shows the nonuniform distribution of craters with evidence for liquid water. Because we only survey craters that

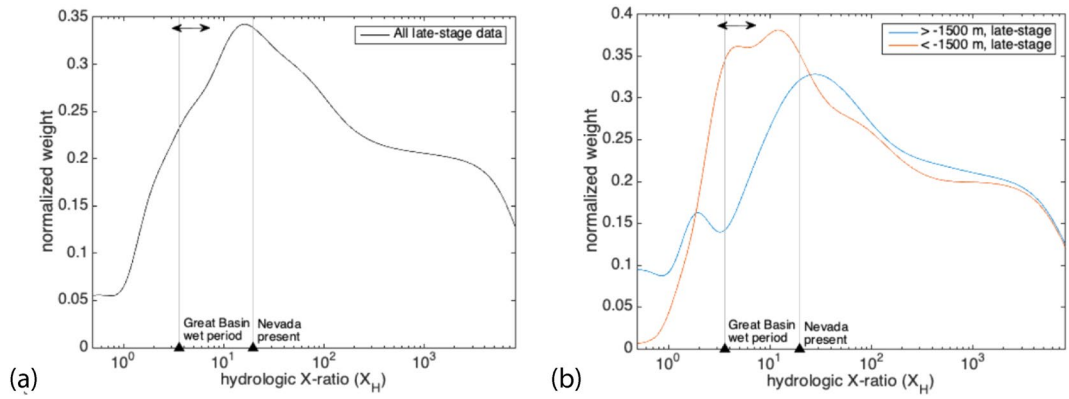

Figure 3. Kernel-density estimates of late-stage aridity. The aridity that we estimated from late-stage geologic proxies is overall greater than that for early-stage rivers: double-headed arrows at top of plot correspond to Matsubara et al. (2011) estimate for early-stage rivers, $X_{H,ancient} = 5 \pm 2$. (a) Overall aridity increases with time. (b) High elevations dried out sooner. Here, paleo-aridity is assumed to simultaneously satisfy both geomorphic aridity upper limits and geomorphic aridity lower limits recorded within the same basin. Modern-Earth aridity values shown by black triangles are from Matsubara et al. (2011; for Western Nevada). Log-uniform prior on $X_H = \{0.1, 10^4\}$; Figure S7 in Supporting Information S1 shows sensitivity test.

formed relatively recently (Tanaka et al., 2014), our survey provides strong evidence that relatively recent rivers/lakes were more frequent at off-equatorial latitudes (Figure 2b; Wilson et al., 2021). Lower-lying craters more frequently show evidence for past rivers/lakes (Figure S6b in Supporting Information S1; Kite et al., 2022).

Figures 3 and 4 sum up survey results. Typical X_H was 7–38 (median fan terminus constraint to median lake deposit constraint), corresponding to arid-to-hyperarid conditions, with deltas and overspill channels recording semiarid conditions (median $X_H = 4$). This is more arid than that reported for early lakes (by, e.g., Matsubara et al. (2011)), $X_{H,ancient} = 5 \pm 2$, and is similar to that of modern Western Nevada ($X_H = 19.7$ according to Matsubara et al. (2011)). In the southern midlatitudes (high ground), late-stage $X_H < 10$ is less common south of 10°S (Figure 4)—in other words, there is very little evidence for conditions moister than modern Nevada. By contrast, in the northern midlatitudes and at the equator (lower ground), the break-in-slope elevations of scarp-fronted deposits interpreted as deltas (filled blue diamonds in Figure 4) indicate relatively big lakes. The difference between hemispheres gives a p-value of 0.002, and $X_H < 10$ is found mostly at $<-1{,}500$ m elevation ($p = 0.01$). In summary, at high elevations, the central aridity estimate is more arid than modern Nevada. At lower elevations, some locations were less arid than modern Nevada (at least intermittently), similar to aridity estimates for the earlier-stage river era.

4. Aridity Change With Time: High and Dry

Late-stage rivers were apparently more spatially patchy than early-stage rivers. Where runoff did occur, we find (on average) a record of more arid climates. For the early-stage lakes (~3.6 Ga), Matsubara et al. (2011) report $X_{H,ancient} = 5 \pm 2$. This is comparable to the X_H for the U.S. Great Basin wet period ~20 Kya ($X_H \approx 3.5$ according to Matsubara et al. (2011)). These data indicate a climate trend, to more arid climate (our preferred explanation), or alternatively toward briefer wet events (disfavored by our data, Supporting Information S1), on global average. Southern midlatitudes show a shift over time toward smaller lakes, but intermittent wet climates (semiarid to arid) persisted near the equator and in the northern midlatitudes. Considering only sites with evidence for late-stage aqueous activity, aridity increased greatly at high elevations but only slightly at low elevations (Figure 5). Similar X_H at low elevations during the Noachian through Amazonian is consistent with the paucity of late-stage low-latitude lake overspills (Goudge et al., 2016). The high-relief rims of the young craters surveyed in this study make overspill more difficult for a given X_H than for the more muted rims of ancient craters.

Intriguingly, Stucky de Quay et al. (2020)'s analysis of early-stage lake overspills shows (their Figure 4) the strongest requirements for humid conditions at high elevation (Figure S9 in Supporting Information S1). Stucky de Quay et al. (2020)'s 96-paleolake data set consists of "hydrological systems in which the morphologies indicated precipitation as a main water source, either as rain or snow […] open-basin and closed-basin lakes fed by dendritic valley networks with a main trunk having a Strahler order of ≥3" (the less selective data set of Fassett

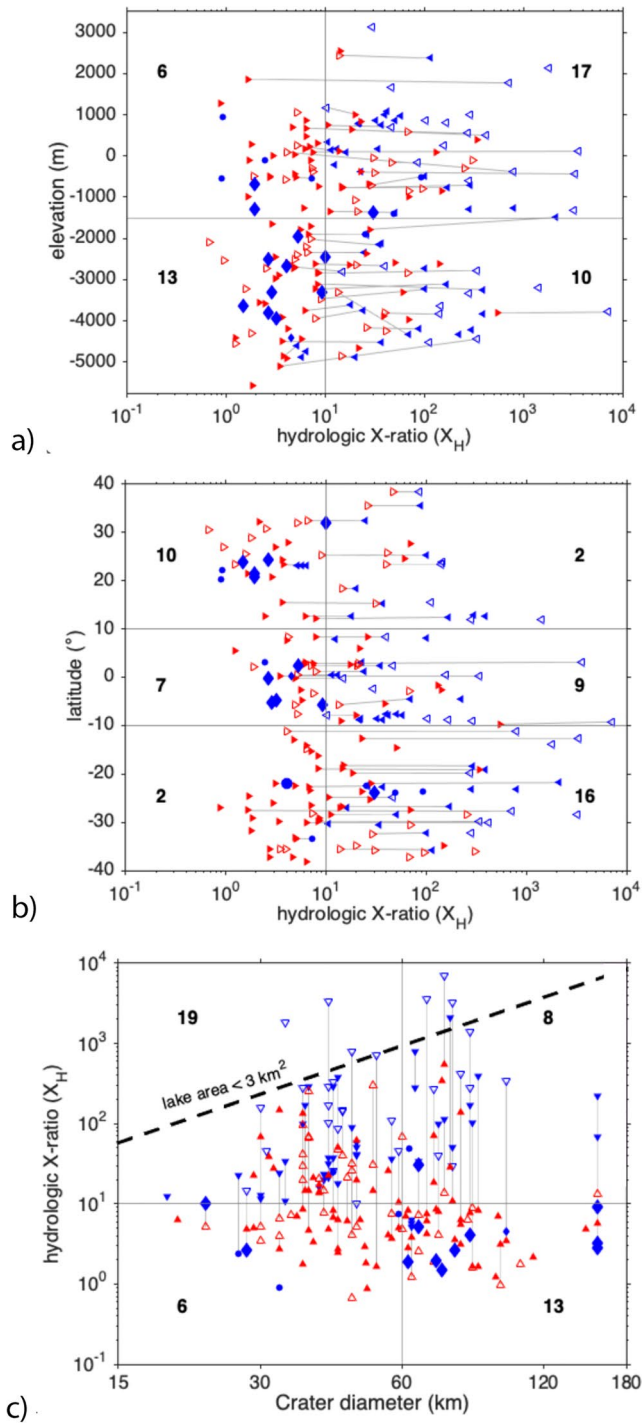

Figure 4. Late-stage aridity constraints. Blue triangles are upper limits on aridity (e.g., lake deposit extent), red triangles are lower limits on aridity (e.g., from alluvial fan termini), and blue diamonds are best-estimates of lake elevation (e.g., from a delta top). (a) X_H versus elevation. Blue triangles = FCBDs (interpreted as lake deposits; unfilled = candidate), blue diamonds = deltas/shorelines, blue circles = internal spillways, red filled triangles = alluvial fan toes, and red unfilled triangles = channel-stops. Numbers correspond to the number of constraints lying entirely inside a rectangular region. Gray lines connect lowest and highest constraints for a single basin. (One −7,500 m data point is cropped). (b) X_H versus latitude. (c) X_H versus crater diameter. Black dashed line highlights where small lake deposits might be missed by survey.

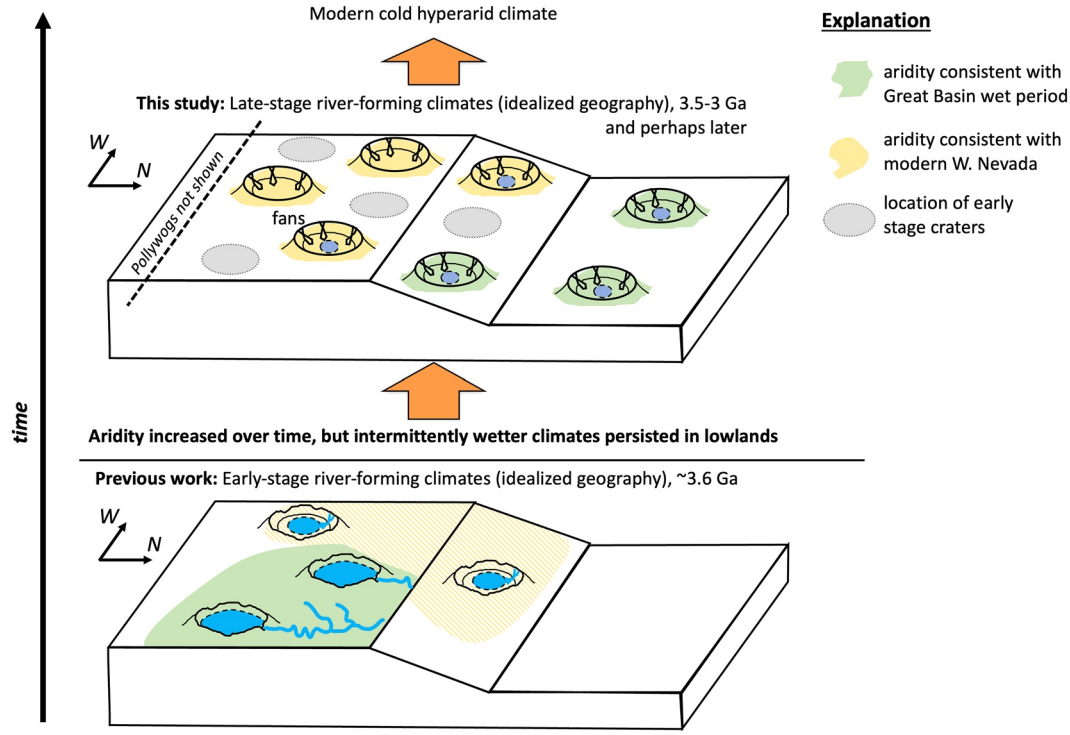

Figure 5. Graphic summary of results.

and Head (2008) shows only a weak trend toward more-humid conditions at high elevation). Stucky de Quay et al. (2020)'s result is the opposite of our late-stage result, suggesting a reversal of the elevation dependence of *X*-ratio as Mars evolved.

5. Discussion and Conclusions

The late-stage trend to higher X_H at high elevation (Figure 3) can be explained by a change in the strength of greenhouse warming over time, such that highlands became almost always too cold for liquid water (Kite et al., 2022). In this scenario, higher-elevation lakes would have less meltwater runoff. Alternatively, in a very-warm-climate scenario (too warm for ground ice), if infiltration became an important water sink for lakes, then high lakes would lose water while water would upwell at low elevations. Thus, a decline in Mars' groundwater table (e.g., Andrews-Hanna & Lewis, 2011; Jakosky, 2021; Salese et al., 2019) might also explain Figure 3 trends. A third possibility is that water vapor was sourced from evaporation at very low elevations, and that highlands were most horizontally distant from the water source and therefore water-starved (Turbet & Forget, 2019). We favor the snow/ice-melt explanation because snow/ice-melt can be patchy and the late-stage erosion is patchy. Snow/ice-melt is consistent with evidence for equatorial thermokarst (Warner et al., 2010).

In the future, measurements of the grain size of clasts moved by late-stage rivers might be decisive in distinguishing between the drying-while-warm versus drying-while-cool scenarios for Mars. At Gale crater, the rover *Curiosity* has encountered proxies for aridity such as mudcracks (Stein et al., 2018). Our data include late-stage Gale lakes (Palucis et al., 2016), conceivably preserved at Gediz Vallis ridge. Thus *Curiosity*'s traverse may allow ground-truthing of the scenario in Figure 5.

Our results reinforce the interpretation (e.g., Irwin et al., 2015) that a hydrologic cycle fueled late-stage rivers. River/lake sediments found within large "host" impact craters often encapsulate smaller impact craters, which today appear partially exhumed (Table S1 in Supporting Information S1). In order for these smaller craters to accumulate, a time interval of ≥0.2 Gyr between the formation of the "host" craters and the end of river activity is required. This disproves the hypothesis (Mangold et al., 2012) that these rivers were triggered by the energy of the impact that formed the "host" crater. This is because ≥0.2 Gyr is too long for the energy of the

"host"-crater-forming impact to contribute to fan formation (Kite et al., 2017; Table S2 in Supporting Information S1). The distribution of X_H with crater size suggests wet events lasting at least decades (Supporting Information S1), consistent with the steady state assumption made here.

The northern hemisphere X_H permits a late-stage ocean, consistent with some models (e.g., Di Achille & Hynek, 2010; Schmidt et al., 2022). However, the case for a Mars ocean remains equivocal: delta locations suggest deltas drained into large lakes, not an ocean (e.g., Rivera-Hernández & Palucis, 2019).

Mars has many relatively young exit-breach craters or "pollywogs" (Wilson et al., 2016). Almost all are omitted from of our study, because of their small size and location poleward of 40°. Pollywog overspill (Warren et al., 2021) would suggest $X_H < 1$, very different from the aridity of the low/midlatitudes, or, alternatively, groundwater release. It also remains to be determined whether late-stage lake overspills in Valles Marineris (e.g., Warner et al., 2013) match the within-crater X_H pattern (Figure 4).

A limitation of our study is that we do not distinguish between playas and perennial lakes. However, if smaller lakes dried up seasonally, then that would make the annual-average climate even more arid than reported here, and accentuate the "high-and-dry" pattern, so this limitation is not severe.

In summary, a globally distributed survey of paleohydrologic proxies for late-stage river-forming climates (Figures 1 and 2), when compared to previous work on early-stage river-forming climates (Figure 3), indicates a climate trend, to more arid climate (our preferred explanation), or, alternatively, toward briefer wet events (disfavored by data; Supporting Information S1). Southern midlatitudes show a shift toward smaller lakes over time, but intermittent wetter climates persisted near the equator and in the northern midlatitudes. These results sharpen our view of Mars' wet-to-dry transition, but overall, it is surprising that this major environmental catastrophe remains so poorly understood. The challenge to models of Mars' climate (e.g., Guzewich et al., 2021; Kamada et al., 2021; Kite et al., 2021; Turbet & Forget, 2021) and climate evolution (e.g., Ramirez & Craddock, 2018; Wordsworth et al., 2021) is now to explain these data.

Conflict of Interest

The authors declare no conflicts of interest relevant to this study.

Data Availability Statement

CTX and HiRISE data are available here: https://pds-imaging.jpl.nasa.gov/volumes/mro.html. MOLA data are available here: https://pds-geosciences.wustl.edu/missions/mgs/pedr.html. The files constituting the database, the DTMs generated for this study, and other supporting files are shared using Open Science Framework (osf.io) at https://osf.io/bue4m/ (DOI: https//doi.org/10.17605/OSF.IO/BUE4M; Kite & Noblet, 2022).

Acknowledgments
We thank Lu Pan, Michael Mischna, Susan Conway, Alexandra Warren, and HiWish. We thank Francesco Salese and the other (anonymous) reviewer.

References

Andrews-Hanna, J. C., & Lewis, K. W. (2011). Early Mars hydrology: 2. Hydrological evolution in the Noachian and Hesperian epochs. *Journal of Geophysical Research*, *116*, E02007. https://doi.org/10.1029/2010JE003709

Annex, A. M., & Lewis, K. W. (2020). Regional correlations in the layered deposits of Arabia Terra, Mars. *Journal of Geophysical Research: Planets*, *125*, e2019JE006188. https://doi.org/10.1029/2019JE006188

Davis, J. M., Gupta, S., Balme, M., Grindrod, P. M., Peter, F., Dickeson, Z. I., & Williams, R. M. E. (2019). A diverse array of fluvial depositional systems in Arabia Terra: Evidence for mid-Noachian to early Hesperian rivers on Mars. *Journal of Geophysical Research: Planets*, *124*, 1913–1934. https://doi.org/10.1029/2019JE005976

Di Achille, G., & Hynek, B. M. (2010). Ancient ocean on Mars supported by global distribution of deltas and valleys. *Nature Geoscience*, *3*(7), 459–463. https://doi.org/10.1038/ngeo891

Dickson, J. L., Kerber, L. A., Fassett, C. I., & Ehlmann, B. L. (2018). *A global, blended CTX mosaic of Mars with vectorized seam mapping: A new mosaicking pipeline using principles of non-destructive image editing. Paper presented at Lunar and Planetary Science Conference*. (Vol. 49, pp. 1–2). Lunar and Planetary Institute.

Fassett, C. I., & Head, J. W., III. (2008). Valley network-fed, open-basin lakes on Mars: Distribution and implications for Noachian surface and subsurface hydrology. *Icarus*, *198*(1), 37–56. https://doi.org/10.1016/j.icarus.2008.06.016

Goudge, T. A., Fassett, C. I., Head, J. W., Mustard, J. F., & Aureli, K. L. (2016). Insights into surface runoff on early Mars from paleolake basin morphology and stratigraphy. *Geology*, *44*(6), 419–422. https://doi.org/10.1130/g37734.1

Grant, J. A., Irwin, R. P., III, Grotzinger, J. P., Milliken, R. E., Tornabene, L. L., McEwen, A. S., et al. (2008). HiRISE imaging of impact megabreccia and sub-meter aqueous strata in Holden Crater, Mars. *Geology*, *36*(3), 195–198. https://doi.org/10.1130/g24340a.1

Grant, J. A., & Wilson, S. A. (2011). Late alluvial fan formation in southern Margaritifer Terra, Mars. *Geophysical Research Letters*, *38*(8).

Grotzinger, J. P., Gupta, S., Malin, M. C., Rubin, D. M., Schieber, J., Siebach, K., et al. (2015). Deposition, exhumation, and paleoclimate of an ancient lake deposit, Gale crater, Mars. *Science*, *350*(6257), aac7575. https://doi.org/10.1126/science.aac7575

Guzewich, S. D., Way, M. J., Aleinov, I., Wolf, E. T., Del Genio, A., Wordsworth, R., & Tsigaridis, K. (2021). 3D simulations of the early martian hydrological cycle mediated by a H_2-CO_2 greenhouse. *Journal of Geophysical Research: Planets*, *126*(7), e2021JE006825. https://doi.org/10.1029/2021je006825

Haberle, R. M., Catling, D. C., Carr, M. H., & Zahnle, K. J. (2017). The early Mars climate system. In R. M. Haberle, R. T. Clancy, F. Forget, M. D. Smith, & R. W. Zurek (Eds.), *The atmosphere and climate of Mars* (pp. 497–525). Cambridge University Press.

Holo, S. J., Kite, E. S., Wilson, S. A., & Morgan, A. M. (2021). The timing of alluvial fan formation on Mars. *Planetary Science Journal*, *2*(5), 210. https://doi.org/10.3847/psj/ac25ed

Horvath, D. G., & Andrews-Hanna, J. C. (2017). Reconstructing the past climate at Gale crater, Mars, from hydrological modeling of late-stage lakes. *Geophysical Research Letters*, *44*, 8196–8204. https://doi.org/10.1002/2017GL074654

Irwin, R. P., III, Lewis, K. W., Howard, A. D., & Grant, J. A. (2015). Paleohydrology of Eberswalde crater, Mars. *Geomorphology*, *240*, 83–101. https://doi.org/10.1016/j.geomorph.2014.10.012

Jakosky, B. M. (2021). Atmospheric loss to space and the history of water on Mars. *Annual Review of Earth and Planetary Sciences*, *49*(1), 71–93. https://doi.org/10.1146/annurev-earth-062420-052845

Kamada, A., Kuroda, T., Kasaba, Y., Terada, N., & Nakagawa, H. (2021). Global climate and river transport simulations of early Mars around the Noachian and Hesperian boundary. *Icarus*, *368*, 114618. https://doi.org/10.1016/j.icarus.2021.114618

Kite, E. S. (2019). Geologic constraints on early Mars climate. *Space Science Reviews*, *215*(1), 1–47. https://doi.org/10.1007/s11214-018-0575-5

Kite, E. S., Mischna, M. A., Fan, B., Morgan, A. M., Wilson, S. A., & Richardson, M. I. (2022). Changing spatial distribution of water flow charts major change in Mars's greenhouse effect. *Science Advances*, *8*(21), eabo5894. https://doi.org/10.1126/sciadv.abo5894

Kite, E. S., & Noblet, A. (2022). Data for high and dry: Billion-year trends in the aridity of river-forming climates on Mars. *Open Science Framework*. https://doi.org/10.17605/OSF.IO/BUE4M

Kite, E. S., Sneed, J., Mayer, D. P., & Wilson, S. A. (2017). Persistent or repeated surface habitability on Mars during the late Hesperian-Amazonian. *Geophysical Research Letters*, *44*, 3991–3999. https://doi.org/10.1002/2017GL072660

Kite, E. S., Steele, L. J., Mischna, M. A., & Richardson, M. I. (2021). Warm early Mars surface enabled by high-altitude water ice clouds. *Proceedings of the National Academy of Sciences of the United States of America*, *118*(18), e2101959118. https://doi.org/10.1073/pnas.2101959118

Lamb, M. P., Howard, A. D., Johnson, J., Whipple, K. X., Dietrich, W. E., & Perron, J. T. (2006). Can springs cut canyons into rock? *Journal of Geophysical Research*, *111*, E07002. https://doi.org/10.1029/2005JE002663

Malin, M. C., Bell, J. F., III, Cantor, B. A., Caplinger, M. A., Calvin, W. M., Clancy, R. T., et al. (2007). Context Camera investigation on board the Mars Reconnaissance Orbiter. *Journal of Geophysical Research*, *112*, E05S04. https://doi.org/10.1029/2006JE002808

Mangold, N., Dromart, G., Ansan, V., Salese, F., Kleinhans, M. G., Massé, M., et al. (2020). Fluvial regimes, morphometry, and age of Jezero crater paleolake inlet valleys and their exobiological significance for the 2020 Rover Mission Landing Site. *Astrobiology*, *20*(8), 994–1013. https://doi.org/10.1089/ast.2019.2132

Mangold, N., Kite, E. S., Kleinhans, M. G., Newsom, H., Ansan, V., Hauber, E., et al. (2012). The origin and timing of fluvial activity at Eberswalde crater, Mars. *Icarus*, *220*(2), 530–551. https://doi.org/10.1016/j.icarus.2012.05.026

Matsubara, Y., & Howard, A. D. (2009). A spatially explicit model of runoff, evaporation, and lake extent: Application to modern and late Pleistocene lakes in the Great Basin region, western United States. *Water Resources Research*, *45*, W06425. https://doi.org/10.1029/2007WR005953

Matsubara, Y., Howard, A. D., & Drummond, S. A. (2011). Hydrology of early Mars: Lake basins. *Journal of Geophysical Research*, *116*, E04001. https://doi.org/10.1029/2010JE003739

Matsubara, Y., Howard, A. D., & Gochenour, J. P. (2013). Hydrology of early Mars: Valley network incision. *Journal of Geophysical Research: Planets*, *118*, 1365–1387. https://doi.org/10.1002/jgre.20081

Mayer, D. P., & Kite, E. S. (2016). An integrated workflow for producing digital terrain models of Mars from CTX and HiRISE stereo data using the NASA Ames Stereo Pipeline. Paper presented at 47th Lunar Planetary Science Conference #1241.

McEwen, A. S., Eliason, E. M., Bergstrom, J. W., Bridges, N. T., Hansen, C. J., Delamere, W. A., et al. (2007). Mars Reconnaissance Orbiter's High Resolution Imaging Science Experiment (HiRISE). *Journal of Geophysical Research*, *112*, E05S02. https://doi.org/10.1029/2005JE002605

Moore, J. M., & Howard, A. D. (2005). Large alluvial fans on Mars. *Journal of Geophysical Research*, *110*, E04005. https://doi.org/10.1029/2004JE002352

Morgan, A. M., Howard, A. D., Hobley, D. E., Moore, J. M., Dietrich, W. E., Williams, R. M., et al. (2014). Sedimentology and climatic environment of alluvial fans in the martian Saheki crater and a comparison with terrestrial fans in the Atacama Desert. *Icarus*, *229*, 131–156. https://doi.org/10.1016/j.icarus.2013.11.007

Palucis, M. C., Dietrich, W. E., Williams, R. M., Hayes, A. G., Parker, T., Sumner, D. Y., et al. (2016). Sequence and relative timing of large lakes in Gale crater (Mars) after the formation of Mount Sharp. *Journal of Geophysical Research: Planets*, *121*, 472–496. https://doi.org/10.1002/2015JE004905

Pan, L., Carter, J., Quantin-Nataf, C., Pineau, M., Chauviré, B., Mangold, N., et al. (2021). Voluminous silica precipitated from martian waters during late-stage aqueous alteration. *Planetary Science Journal*, *2*(2), 65. https://doi.org/10.3847/psj/abe541

Ramirez, R. M., & Craddock, R. A. (2018). The geological and climatological case for a warmer and wetter early Mars. *Nature Geoscience*, *11*(4), 230–237. https://doi.org/10.1038/s41561-018-0093-9

Rivera-Hernández, F., & Palucis, M. C. (2019). Do deltas along the crustal dichotomy boundary of Mars in the Gale crater region record a northern ocean? *Geophysical Research Letters*, *46*, 8689–8699. https://doi.org/10.1029/2019GL083046

Salese, F., Kleinhans, M. G., Mangold, N., Ansan, V., McMahon, W., De Haas, T., & Dromart, G. (2020). Estimated minimum life span of the Jezero fluvial delta (Mars). *Astrobiology*, *20*(8), 977–993. https://doi.org/10.1089/ast.2020.2228

Salese, F., Pondrelli, M., Neeseman, A., Schmidt, G., & Ori, G. G. (2019). Geological evidence of planet-wide groundwater system on Mars. *Journal of Geophysical Research: Planets*, *124*, 374–395. https://doi.org/10.1029/2018JE005802

Schmidt, F., Way, M. J., Costard, F., Bouley, S., Séjourné, A., & Aleinov, I. (2022). Circumpolar ocean stability on Mars 3 Gy ago. *Proceedings of the National Academy of Sciences of the United States of America*, *119*(4), e2112930118. https://doi.org/10.1073/pnas.2112930118

Smith, D. E., Zuber, M. T., Frey, H. V., Garvin, J. B., Head, J. W., Muhleman, D. O., et al. (2001). Mars Orbiter Laser Altimeter: Experiment summary after the first year of global mapping of Mars. *Journal of Geophysical Research*, *106*(E10), 23689–23722. https://doi.org/10.1029/2000JE001364

Stein, N., Grotzinger, J. P., Schieber, J., Mangold, N., Hallet, B., Newsom, H., et al. (2018). Desiccation cracks provide evidence of lake drying on Mars, Sutton Island member, Murray formation, Gale Crater. *Geology*, *46*(6), 515–518. https://doi.org/10.1130/g40005.1

Stucky de Quay, G., Goudge, T. A., & Fassett, C. I. (2020). Precipitation and aridity constraints from paleolakes on early Mars. *Geology*, *48*(12), 1189–1193. https://doi.org/10.1130/g47886.1

Tanaka, K. L., Skinner, J. A., Jr., Dohm, J. M., Irwin, R. P., III, Kolb, E. J., Fortezzo, C. M., et al. (2014). Geologic map of Mars. In *U.S. Geological Survey Scientific Investigations Map 3292* (scale 1:20,000,000, pamphlet, p. 43). https://doi.org/10.3133/sim3292

Tebolt, M., & Goudge, T. A. (2022). Global investigation of martian sedimentary fan features: Using stratigraphic analysis to study depositional environment. *Icarus*, *372*, 114718. https://doi.org/10.1016/j.icarus.2021.114718

Turbet, M., & Forget, F. (2019). The paradoxes of the Late Hesperian Mars ocean. *Scientific Reports*, *9*(1), 1–5. https://doi.org/10.1038/s41598-019-42030-2

Turbet, M., & Forget, F. (2021). 3-D global modelling of the early martian climate under a dense $CO_2 + H_2$ atmosphere and for a wide range of surface water inventories. arXiv:2103.10301.

Wang, C. Y., Manga, M., & Wong, A. (2005). Floods on Mars released from groundwater by impact. *Icarus*, *175*(2), 551–555. https://doi.org/10.1016/j.icarus.2004.12.003

Warner, N., Gupta, S., Kim, J. R., Lin, S. Y., & Muller, J. P. (2010). Hesperian equatorial thermokarst lakes in Ares Vallis as evidence for transient warm conditions on Mars. *Geology*, *38*(1), 71–74. https://doi.org/10.1130/g30579.1

Warner, N. H., Sowe, M., Gupta, S., Dumke, A., & Goddard, K. (2013). Fill and spill of giant lakes in the eastern Valles Marineris region of Mars. *Geology*, *41*(6), 675–678. https://doi.org/10.1130/g34172.1

Warren, A. O., Holo, S., Kite, E. S., & Wilson, S. A. (2021). Overspilling small craters on a dry Mars: Insights from breach erosion modeling. *Earth and Planetary Science Letters*, *554*, 116671. https://doi.org/10.1016/j.epsl.2020.116671

Whipple, K. X., Snyder, N. P., & Dollenmayer, K. (2000). Rates and processes of bedrock incision by the Upper Ukak River since the 1912 Novarupta ash flow in the Valley of Ten Thousand Smokes, Alaska. *Geology*, *28*(9), 835–838. https://doi.org/10.1130/0091-7613(2000)028<0835:rapobi>2.3.co;2

Wilson, S. A., Howard, A. D., Moore, J. M., & Grant, J. A. (2016). A cold-wet middle-latitude environment on Mars during the Hesperian-Amazonian transition: Evidence from northern Arabia valleys and paleolakes. *Journal of Geophysical Research: Planets*, *121*, 1667–1694. https://doi.org/10.1002/2016JE005052

Wilson, S. A., Morgan, A. M., Howard, A. D., & Grant, J. A. (2021). The global distribution of craters with alluvial fans and deltas on Mars. *Geophysical Research Letters*, *48*, e2020GL091653. https://doi.org/10.1029/2020GL091653

Wordsworth, R., Knoll, A. H., Hurowitz, J., Baum, M., Ehlmann, B. L., Head, J. W., & Steakley, K. (2021). A coupled model of episodic warming, oxidation and geochemical transitions on early Mars. *Nature Geoscience*, *14*(3), 127–132. https://doi.org/10.1038/s41561-021-00701-8

References From the Supporting Information

Goddard, K., Warner, N. H., Gupta, S., & Kim, J. R. (2014). Mechanisms and timescales of fluvial activity at Mojave and other young Martian craters. *Journal of Geophysical Research: Planets*, *119*, 604–634. https://doi.org/10.1002/2013JE004564

Lewis, K. W., Aharonson, O., Grotzinger, J. P., Kirk, R. L., McEwen, A. S., & Suer, T. A. (2008). Quasi-periodic bedding in the sedimentary rock record of Mars. *Science*, *322*(5907), 1532–1535. https://doi.org/10.1126/science.1161870

Michael, G. G. (2013). Planetary surface dating from crater size-frequency distribution measurements: Multiple resurfacing episodes and differential isochron fitting. *Icarus*, *226*(1), 885–890. https://doi.org/10.1016/j.icarus.2013.07.004

Steele, L. J., Kite, E. S., & Michaels, T. I. (2018). Crater mound formation by wind erosion on Mars. *Journal of Geophysical Research: Planets*, *123*, 113–130. https://doi.org/10.1002/2017JE005459